Real Time Reconstruction of Radio Environment Maps in Indoor Millimeter-Wave Beamforming with Beam Changes

Takumi Bushi*, Toshiro Nakahira†, Shoko Shinohara†, Yusuke Asai†, Kenji Ohira‡, and Hideyuki Shimonishi‡
*Graduate School of Information Science and Technology,
Osaka University, Osaka, Japan
Email: bushi.takumi@ist.osaka-u.ac.jp
*NTT Access Network Service Systems Laboratories,
Nippon Telegraph and Telephone Corporation, Yokosuka, Japan
Email: toshirou.nakahira@ntt.com, shoko.shinohara@ntt.com, yusuke.asai@ntt.com
‡Cybermedia Center,
Osaka University, Osaka, Japan
Email: ohira.kenji.oict@osaka-u.ac.jp, shimonishi.cmc@osaka-u.ac.jp

***Abstract*—To enable robust wireless communications towards the future Cyber Physical System by optimizing beamforming in real time, it is essential to quickly estimate changes in the radio environment map (REM) after altering the beam direction. In addition, because of the difficulty to predict detailed REMs with high accuracy, especially for millimeter waves, a probabilistic REM, which estimates the radio signal strength at any point as a probability distribution rather than as a deterministic value, is expected. In this paper, to enable fast and probabilistic REM estimation, we propose a scheme that divides the estimation formula into a linear term and a Gaussian Process Regression (GPR) term to minimize the recalculation time associated with beam adjustments. We also propose a GPR kernel that uses polar coordinates centered on the base station angle to better capture the characteristics of narrow beams like millimeter waves. We evaluated the proposed scheme using Kullback-Leibler Divergence (KLD) to compare the measured and estimated distributions of the radio signal strength. In the REM estimation after beam adjustment, an accurate distribution is estimated at 29 out of 35 points with a KLD of 0.5 or lower. The proposed method achieved approximately 50 times faster REM reconstruction compared to a simple REM using GPR, enabling dynamic beam-forming optimization in mm-wave environment.**

***Index Terms*—Radio Environment Maps, mm-wave, Cyber-Physical Systems, Beamforming, Gaussian Process Regression**

I. Introduction

Research on Cyber Physical Systems (CPS) is actively progressing toward a future advanced society, where remote controlled robots, drones, and cars co-exist with humans and help each other safely and efficiently. In these systems, robots acquire information about their surroundings via wireless communication, and control is carried out based on that information, thus stable wireless communication is crucial. If wireless communication is disrupted for any reason, there is a risk that robots may behave unexpectedly or remote operations may be interrupted, posing potential dangers to both humans and robots. Therefore, it is expected that active network control, such as beamforming [1], will optimize radio conditions according to robot movements.

To provide stable wireless communication at all times in any situation, it is important to accurately understand the geographical condition of radio communication in the area, which is called Radio Environment Maps (REM), or the digital twin of the radio communication environment. In addition, there is another digital twin that represents a real space where robots and humans collaborate. By combining these digital twins, a safe remote robot control becomes available. However, because of constraints such as sensor placement and costs, it is not realistic to directly observe the radio conditions of the entire area. Therefore, there have been many studies to estimate the radio wave conditions in the entire area based on data acquired from a part of the area [2]–[10]. However, in a dynamic beamforming environment, it is still challenging to estimate the REM after changing the beam in real time.

The use of millimeter waves to collect large amounts of real-time information from sensors (such as LiDAR and high-resolution cameras) makes REM estimation even more difficult. In millimeter wave communications, the strength of the received signal is significantly affected even by a few centimeters of difference in the location of the terminal device and the orientation of its antenna. Since predicting detailed REMs with high accuracy is unrealistic in such an environment, we discuss *Probabilistic REM*, which gives a probability distribution of the signal strength at arbitrary points on a map, rather than a deterministic value. The variance of the distribution indicates the stability of the signal strength and the certainty of the estimations. Thus, probabilistic REM allows for robust estimation of the wireless radio environment by analyzing the tail of the probability distribution of the predicted radio strength.

The probabilistic representation of digital twins, introduced in [11], for both REM and real space work together and

978-3-903176-66-9

help to improve the robustness of CPS. For example, a robot can avoid a path where the signal strength is estimated to be high but its variance is wider and choose a path where the variance is small. On the other hand, if we look at computational complexity, probabilistic REM requires a large computational effort for probability calculations, and real-time calculations are not easy. Therefore, in this paper, we propose a method for real-time reconstruction of REMs in millimeter wave environment with dynamic beamforming. Specifically, the objectives of our study are as follows:

- Proposing a method that allows for fast recalculation of the REM in response to changes in the beam direction.
- Proposing a method that provides prediction intervals to account for differences in terminal orientation and movements of a few centimeters.

To meet these requirements, we propose a probabilistic REM estimation method that divides the estimation formula into a linear term and a GPR (Gaussian Process Regression) term. When the beam direction is changed, only the linear terms are recalculated, allowing fast REM updates. The GPR term, on the other hand, gives the probability distribution of the signal strength and is fixed for the beam direction. We also propose a GPR kernel based on an Automatic Relevance Determination (ARD) inspired by an angular coordinate system centered on the direction the base station is facing, rather than using Euclidean distances in a Cartesian coordinate system. In general, GPR assumes that the closer two points are in space, the higher the correlation. However, in millimeter waves, this correlation is not uniform in any direction in space, and different correlations are observed on the axis of base station orientation and on the orthogonal axis. This approach addresses the directivity of millimeter waves and the characteristics of LOS/NLOS. In the following, we briefly describe related work and then our proposed method, followed by the measurement results obtained from our in-door millimeter wave private 5G system, and finally experimental evaluation results for the proposed REM estimation method.

II. Related Work

There are so many studies that estimate the REM of the entire area. For example, some studies proposed methods to estimate REM based on the distance from access points (AP) and the strength of radio waves at the observation points [2], [3]. Such methods enable understanding of radio wave conditions, which can be used for the control of robot operations and the design of communication areas. GPR has been used in previous REM research to provide prediction intervals [4]–[6]. In [4], a method is proposed to recursively estimate REM in situations where measurement data are continuously added. In [5], a technique is proposed that applies GPR within clusters, created using k-means clustering, to reduce the computational cost of constructing the overall REM. In [6], a method is proposed for generating REM using deep Gaussian processes to address cases where measurement data are sparse. In [7], an attempt was made to separate the overall trends of radio waves from the effects of spatial shadow fading. A log-path model and a GPR with distance as input were used for the overall radio wave trends. In addition, GPR was used for spatial shadow fading. A method for estimating probabilistic REM using MRF (Markov Random Field) is proposed in [8]. The model can arbitrarily describe correlations between any points and thus can capture the structure of the space such as LOS/NOS. However, MRFs, especially those with closed loops, are computationally expensive and difficult to recalculate in real time. REM can also predict the signal spectrum in a target area and help to manage the spectrum data [9], [10]. In [9], it was demonstrated how the spectrum map predicts channel performance metrics, such as channel capacity, spectral efficiency, and secondary throughput. As mentioned above, there have been many studies in the past to estimate the REM, some of which explicitly aim to obtain it probabilistically. However, it remains challenging to both obtain the probability distribution and recalculate it quickly when the beam direction is changed.

III. REM Estimation Method

A. Overview

In this paper, millimeter wave radios are expressed in probabilistic REM to take into account their spatio-temporal variations. If these variations are viewed as a distribution, the shape of the distribution is affected by various factors, such as noise, fading, fluctuations of receivers, etc. We took into account temporal and spatial variations in our measurements and obtained a distribution that is nearly Gaussian, as shown in the next section. Therefore, in this paper, we use a normal distribution and employ GPR to derive probabilistic REM.

To allow fast recalculation and probabilistic estimation, the proposed method divides the estimation of REM into two components, namely a linear term L, which is affected by the angle of beam radiation, and a GPR term G, which is not affected, as shown in the following equation:

$$P(l_T, b) \sim \mathcal{N}(L(l_T, b) + G(l_T), \sigma_G^2(l_T)), \tag{1}$$

where l_T and b represent the 3D position of the terminal and the angle of the beam, respectively.The linear term L represents the radio wave conditions considering the distance attenuation and the angle from the beam center, while the GPR term G primarily accounts for spatial factors such as fading and provides probability distributions. The linear term L includes b as a variable, while the GPR term G does not; therefore, by limiting the recalculation to only the linear term L when the beam changes, the computational load is minimized. To address the directivity of millimeter waves, we denote the 3D location of a terminal $\mathbf{l_T}$ as (ρ, θ, ϕ) in polar coordinates centered on the location and orientation of the base station, as shown in Fig. 1. ρ is the distance between $\mathbf{l_T}$ and the base station. θ and ϕ are the angle between the orientation of the base station and the orientation to the terminal, and the rotation around the axis, respectively.

B. Linear Term

The linear term is used to describe the overall characteristics of the space, which is affected by the angle of the beams. The linear term is expressed as a function based on the log-scale distance between the antenna and the terminal, and the angle between them. If there are multiple beams, the smallest angle is used. Based on our preliminary experiments, we found that the linear term expressed as the following equation largely fits the measurement results.

$$L(l_T, b) = \beta_0 - 20\beta_1 \log(\rho) - \beta_2 \angle(b, l_T) \tag{2}$$

Here, $L(b, l_T)$ denotes the signal strength in dBm at l_T assuming the absence of interference factors such as fading. b and $\angle(b, l_T)$ are the direction in which the base station is facing, and the angle between b and the direction to the terminal, respectively. When multiple beams are present, the smallest angle is used. The parameters β_0, β_1, and β_2 are intended to be solved using multiple regression analysis using measurement data obtained by experiments.

C. GPR Term

The GPR term primarily accounts for spatio-temporal factors such as noise, fading, fluctuations of receivers, etc. For Gaussian Process (GP), the input variables are the data measurement positions, and the output variables are the values obtained by subtracting the linear term $L(b, l_T)$ from the measured RSRP (Reference Signal Received Power), so that the sum of the Linear and GPR terms express the original REM. This includes data measured in both the LOS and the NLOS areas. As a result, the output values of the GPR term at the LOS locations will be nearly zero with some measurement errors, while at locations with significant spatial shadow fading, such as NLOS, the values will be large.In this study, we employ GPR to take into account the instability and error of radio measurements. In existing studies, data from each location were used as input data one at a time, which did not account for the variations in the received signal strength at each location. To address significant variations due to the characteristics of millimeter wave, we conducted measurements at varying spatio-temporal locations by placing a measurement terminal on a turntable and trained the GPR model with varying sample data. Using multiple measurement data points around location l as training data D_l(e.g. $D_1, \ldots, D_M$), this approach addresses the variations due to differences in terminal orientation and small positional changes that are prominent in millimeter waves. For any natural number N, we define the output vector $\mathbf{f}$ corresponding to the inputs $\mathbf{l}_1, \mathbf{l}_2, \ldots, \mathbf{l}_N \in \mathcal{L}$ as follows:

$$\mathbf{f} = (f(\mathbf{l}_1), f(\mathbf{l}_2), \ldots, f(\mathbf{l}_N)), \tag{3}$$

where each input $\mathbf{l}_i$ represents a 3D location in the space $\mathcal{L}$, and $\mathcal{L}$ denotes the set of all possible 3D locations. The GPR model uses these 3D locations as inputs to predict the corresponding outputs $\mathbf{f}$. Assuming that the observations are subject to noise, the observation model can be expressed as:

$$D_n = f(\mathbf{l}_n) + \epsilon_n, \tag{4}$$

where ϵ_n is the observation noise, typically Gaussian with mean 0 and variance σ^2_{obs}.

$$K'(\mathbf{l}_n, \mathbf{l}_{n'}) = k(\mathbf{l}_n, \mathbf{l}_{n'}) + \sigma^2_{\text{obs}} \delta_{nn'}, \tag{5}$$

where $k(\mathbf{l}_n, \mathbf{l}_{n'})$ is the kernel function, and $\delta_{nn'}$ is the Kronecker delta. Thus, the Gaussian process $\mathcal{GP}$ is expressed as follows (assuming a mean function $m(\mathbf{l}) = 0$):

$$\mathbf{f} \sim \mathcal{GP}(0, K'(\mathbf{l}, \mathbf{l}')). \tag{6}$$

Given the observed data D, the conditional distribution of D follows a normal distribution with the predicted mean G^* and the predictive variance σ^{*2}_G, calculated based on the Gaussian process model with the following equations.

$$\begin{aligned} &G^* = \mathbf{k}_*^\top \mathbf{K}^{-1} D, \quad \sigma^{*2}_G = k_{**} - \mathbf{k}_*^\top \mathbf{K}^{-1} \mathbf{k}_* \\ &\mathbf{k}_* = (k(\mathbf{l}^*, \mathbf{l}_1), k(\mathbf{l}^*, \mathbf{l}_2), \ldots, k(\mathbf{l}^*, \mathbf{l}_N))^\top, \quad k_{**} = k(\mathbf{l}^*, \mathbf{l}^*). \end{aligned} \tag{7}$$

Using these equations, $G(l_T)$ and $\sigma^2_G(l_T)$ can be calculated as G^* and σ^{*2}_G, respectively.

In this study, we propose a GPR kernel inspired by polar coordinates to better capture the characteristics of narrow beams like millimeter wave. In the kernel, the features of the 3D location $\mathbf{l}$ are divided into two directions, one in which the base station is facing and the other orthogonal to it. Assuming that the correlations of spatial shadow fading in these directions follow a normal distribution, the kernel uses the RBF (Radial Basis Function) kernel.

$$kernel(\mathbf{l}, \mathbf{l}') = \sigma^2 \exp\left(-\frac{p^2}{2L_1}\right) \exp\left(-\frac{q^2}{2L_2}\right), \tag{8}$$

where p and q are distances in two directions, one the base station facing and the other orthogonal to it, respectively, as shown in Fig. 1. L represents the length scales for each direction, indicating how quickly the correlation between points decreases as the distance increases. σ is the scale parameter of the kernel that controls the amplitude of the predicted output of the model. The locations $\mathbf{l}$ and $\mathbf{l}'$ are denoted as (ρ, θ, ϕ) and (ρ', θ', ϕ'), respectively, in the polar coordinates centered on the base station, and thus the distances p and q between them in their directions are defined as follows:

$$p = |\rho \cos(\theta) - \rho' \cos(\theta')| \tag{9}$$

$$q = \sqrt{(\rho \sin(\theta)\cos(\phi) - \rho' \sin(\theta')\cos(\phi'))^2 + (\rho \sin(\theta)\sin(\phi) - \rho' \sin(\theta')\sin(\phi'))^2}. \tag{10}$$

Different length-scales L_1 and L_2 are used for each direction. This allows the model to apply different correlations for these directions. In the direction the base station is facing, the RSRP values are close because the base station side of the LOS location is, by definition, also an LOS location. Similarly, the values are close in the direction opposite to the base station at the NLOS location, which by definition is also an NLOS location. However, its orthogonal direction does not exhibit such properties. Therefore, the correlation in the direction the base station is facing tends to be relatively high, whereas the correlation in its orthogonal direction tends to be relatively

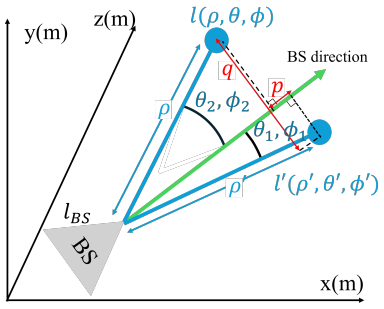

Fig. 1. Distance used in the kernel

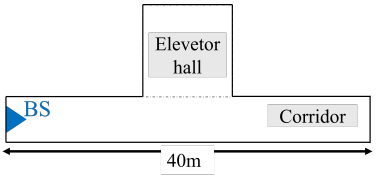

Fig. 2. The condition of indoor structures

low. This kernel allows for the appropriate capture of the effects of spatial structures.

D. Evaluation of Probability Distribution Using KLD

Since the proposed method obtains the REM as a probability distribution, an evaluation measure is necessary for this purpose. Furthermore, in order to evaluate how well the estimate obtained as a normal distribution fits the actual distribution, it is necessary to evaluate not only the mean and variance, but also the shape of the distribution. Therefore, we propose to evaluate them using the Kullback-Leibler Divergence (KLD). KLD indicates the divergence between the estimated probability distribution of the RSRP and the actual distribution. Therefore, when the estimation accuracy is high, the KLD value will be small. The formula is expressed as follows.

$$D_{KL}(P \parallel Q) = \sum_i P(i) \log \frac{P(i)}{Q(i)} = \mathbb{E}_P \left[\log \frac{P(i)}{Q(i)} \right] \quad (11)$$

Here, $P(i)$ and $Q(i)$ are the probabilities that the values of the random variables following the probability distributions P and Q, respectively, are i. P represents the distribution of the measured data itself and Q represents the predicted values of P. By this definition, the KLD cannot be less than 0.

IV. Radio Measurement

A. Environment Description

We conducted an experiment in a real-life environment, measuring the RSRP multiple times at arbitrary indoor points, as shown in Fig. 2. The floor is mainly composed of a corridor and an elevator hall. The corridor is approximately 40 meters long and the elevator hall is 20 meters from the base station. The elevator hall is in the NLOS area. In this measurement, the measurement terminal is placed on a turntable and rotated during measurement, as shown in Fig. 3. This rotation causes

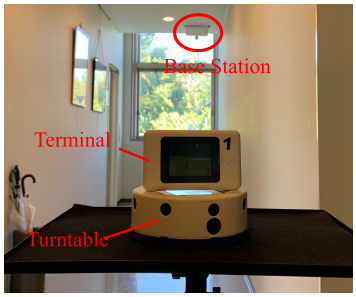

Fig. 3. Measurement devices and methods

the blocking of radio waves by the terminal's frame to vary, and as the position changes by several centimeters, the radio environment continuously changes, leading to significant fluctuations in the received signal strength. For each beam angle, measurements were taken at 35 locations, with approximately 120 measurements per location over about 2 minutes. During these measurements, the measurement terminal was placed on the turntable, rotating at at about one revolution per minute.

B. Device Description

The specifications of the base station are shown in Table I. Its location is at the right end of the corridor in Fig. 2, with a height of 2.7 meters and a tilt angle of 8°. As shown in Fig. 4, the base station can configure the beam direction by specifying the assigned beam number. In this measurement, beamforming settings were measured in two scenarios: Static Beamforming Scenario (only beam number 11; downward at an 8°angle) and Dynamic Beamforming Scenario (in addition to beam number 11, beam numbers 29, 47, 65, and 83 are added; downward at angles of 8°, 23°, 38°, 53°, and 68°). The beam settings in the Dynamic Beamforming scenario are configured to reflect the most significant changes in the REM, taking into account the location of the base station. The measurement terminal used was a millimeter wave compatible device, the APAL raku+ [12]. It is capable of measurements in 1 dBm increments within the range of -44 dBm to -140 dBm.

TABLE I
Base Station Specification

Specification	Details
Band	28 GHz (Band n257)
Bandwidth	DL:400MHz (100 MHz x 4 CC),UL:100MHz
Antenna	Directed antenna x64 (8x8)
Half-power angle	V: 13.5, H: 13.5
Transmission power	+8 dBm
Antenna gain	23 dBi
Maximum EIRP	+31 dBm

C. Measurement Results

Figure 5 visualizes the average RSRP values at several points in both the LOS and the NLOS areas. The red points are from the LOS area, and the green points are from the NLOS area. A RSRP value shown in the figure is the average

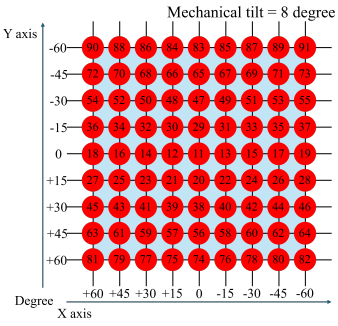

Fig. 4. Beam Directions Configuration Based on Number Assignments

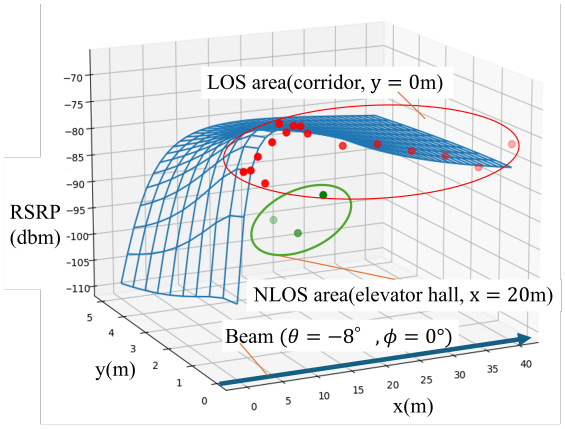

Fig. 5. Prediction based solely on the linear term.

of the series of data measured at the point. In this figure, the base station is located at $(x, y, z) = (0, 0, 2.7)$, and the beam is emitted at a downward angle of 8°. The estimated RSRP values using only the linear term are also shown as a blue surface. It can be observed that the regression is well-fitted for the LOS areas, but the linear term alone fails to account for predictions in NLOS areas.The time series of measured RSRP data at a point is shown in Fig. 6, which exhibits significant fading effects, with continuously changing RSRP values. Since it is virtually impossible to accurately estimate each of these measurement point values, the objective of this study is to estimate these values as a distribution. We also found that, although the variance values were different at various points, the shape of the distribution was almost Gaussian.

V. REM Estimation Results

We perform two types of evaluation of the accuracy of REM. The first evaluation is the Static Beam Scenario, where some measurement data are collected by fixing the beam angle to train the GPR, and then the RSRPs of other points are estimated without moving the beam. In this scenario, we divide the measured data into training and test datasets. The RSRP at the estimation points is predicted from the training data and evaluated by comparing it with the measured data.

The second evaluation is the Dynamic Beamforming Scenario, where the GPR is trained with a particular beam angle,

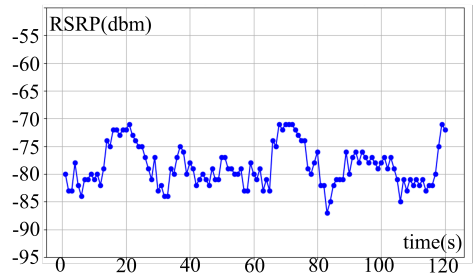

Fig. 6. Changes in RSRP due to small variations in the position or orientation of the device

and then the REM is estimated for other beam angles. In this scenario, measurements are only performed for a particular beam angle obtained in the Static Beam Scenario to train the GPR. Measurements for other beams are performed only for validation, not for training.

A. Shape of Probability Distribution

We first verify the shape of the probability distribution of the RSRPs. Here we train the GPR with all the measurement data obtained for the Static Beam Scenario, and compared the probability distributions obtained by the GPR and by the measurement. The shapes of these distributions are generally consistent. Figure 7 visualizes the measured and estimated probability distributions at the coordinate $(4, 0, 1.8)$ where the KLD is at the median. In this paper, from our measurement results, we consider the agreement between the actual data and the predicted data to be high when the KLD value is between 0.5 and 1, and very high when the KLD value is 0.5 or lower.

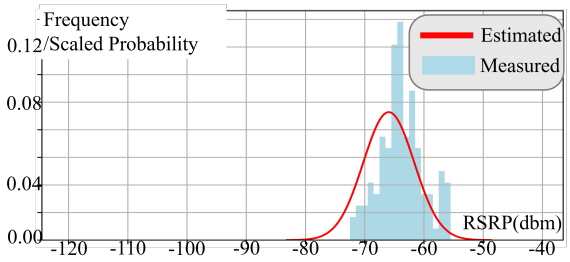

Fig. 7. Estimated and Measured RSRP Distributions When KLD Equals 0.386

B. REM Estimation with Static Beam

In this evaluation, we cross-validated using 1 point out of 35 as validation data and the remaining 34 points as training data, repeating this process for a total of 35 validations. The KLD between the validation data and the estimated values was calculated and is shown in Fig. 8 and Fig. 9. In Fig. 8, the $y = 0$ axis corresponds to the straight corridor, while $y = 2, 3, 4$ corresponds to the locations of the NLOS elevator hall. In the corridor, $x = 0, 1, \ldots, 10$m has measurement data at 1m intervals, and beyond 10m, data is available at 5m intervals, with the corresponding KLD values shown. The

color map in Fig. 8 shows that the KLD values are poor at the points $(x, y) = (1, 0, 1)$ and $(4, 0, 1)$. Although the estimation is poor at the points relatively close to the base station, the estimates at points $(2, 0, 1)$ and $(3, 0, 1)$ are not bad. Therefore, no specific trend related to position was observed in the KLD. Figure 9 shows the histogram of KLD values for each test data and the corresponding estimated data. There were 27 of 35 points where the KLD value was 1 or less and 21 points where the KLD value was 0.5 or less. The estimated REM in the static beam scenario is shown in Fig. 10. This figure shows an average of the distribution as the Estimated RSRP at each location. It is observed that the attenuation is significantly more severe in the elevator hall area, the NLOS locations, and the locations close to the base station but at a large angle to the beam. In all of the area, the RMSE (Rooted Mean Square Error) between the average of the estimated distribution and the average of the measured distribution is 3.28 in this situation.

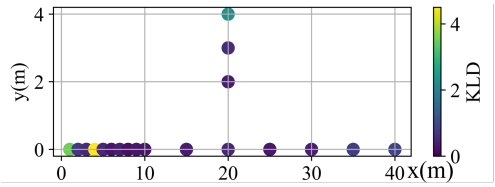

Fig. 8. Positional relationship of KLD (static beam)

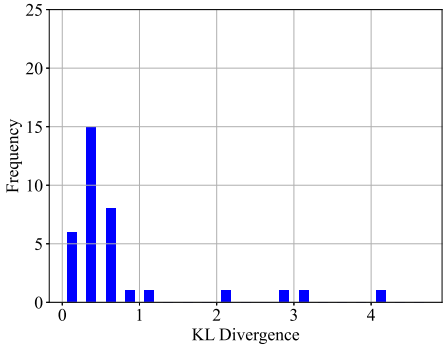

Fig. 9. KLD Distribution (static beamforming)

TABLE II
RMSE OF AVERAGE RSRP AT ALL LOCATIONS

Scenario	RMSE
Static Scenario	3.2
Dynamic Scenario	2.2

C. REM Estimation with Dynamic Beamforming

Using the RSRP data obtained during the beam in the Static Beam Scenario to train the GPR, we estimated the REM for the Dynamic Beamforming Scenario after the beam was changed and compared it with the data measured in the scenario. As

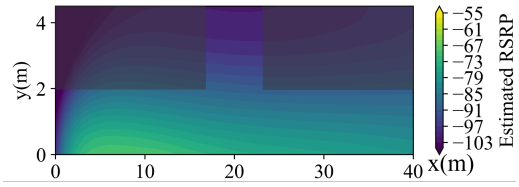

Fig. 10. Estimated REM (static beam)

shown in Figs. 11 and 12, the evaluation was performed using KLD. Of 35 points, 32 had a KLD value of 1 or less. This indicates that the estimation was successful even after the beam was changed, similar to when there was no beam change. However, at the NLOS locations we observed slightly larger KLD values on which we can discuss further improvements.

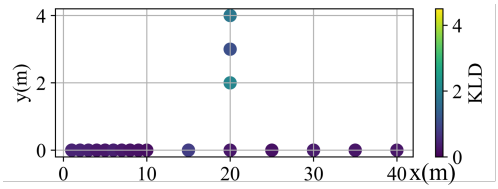

Fig. 11. Positional relationship of KLD (dynamic beamforming)

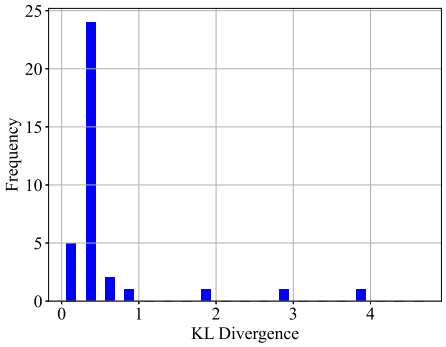

Fig. 12. KLD Distribution (dynamic beamforming)

Figure 13 visualizes the estimated REM, which is the average of the distribution at various locations, during the Dynamic Beamforming Scenario. Compared to REM in Fig. 10, the RSRP within 10 meters of the base station is particularly higher by adding beams pointing to the area. The RMSE between the average of the estimated distribution and the average of the measured distribution is listed in Table. II. In the static scenario, the RMSE was 3.28, and in the dynamic scenario, it was 1.53. This indicates that the REM can be estimated with the same level of accuracy in the dynamic scenario as in the static scenario. Fig. 14 visualizes the comparison between the estimated and actual data at the coordinates$(4, 0, 1.8)$ that were significantly affected by the beam change. It can be seen that the estimated normal distribution is close to the histogram of the actual data.The KLD is 0.29. The average RSRP at

this location is -59.1dB measured and -59.3dB estimated. The calculated values of RSRP obtained with a probability of more than 90% are -63.8 dB and -65.1dB for the measured and estimated values, respectively. Thus, the proposed method is able to accurately estimate RSRPs not only for the average but also for its tail of the distribution, which would greatly help to design radio networks for robust CPS. We can design a remote controlled robot system in which a robot selects a path where the probability of signal strength below -75dB is always less than 10%, for example.

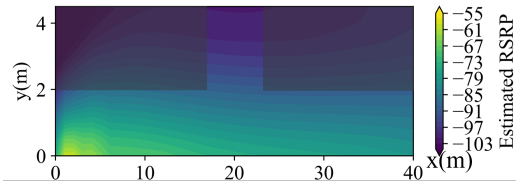

Fig. 13. Estimated REM (dynamic beamforming)

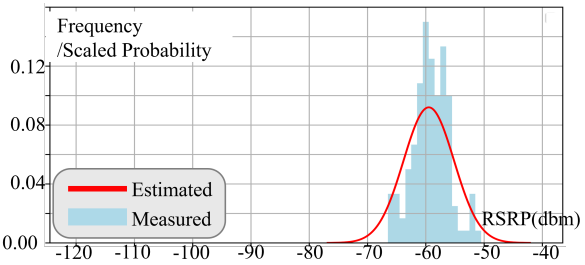

Fig. 14. Estimated and Measured RSRP Distributions when KLD Equals 0.29

D. Evaluation of Computation Times

We compared the speed of the REM reconstruction after a beam change between a simple construction method using GPR and the proposed method. This simple GPR model has the coordinate vector as the explanatory variable and RSRP as the objective variable. In this model, 35 data points are used as training data. REM reconstruction using the simple GPR model involves both training time and inference time. Training time refers to the time taken to adjust the model parameters by fitting the training data, while inference time refers to the time taken to input data into the model and generate the output. The training time for the GPR is $\mathcal{O}(N^3)$ when the number of data points is N, and the inference time for the GPR is $\mathcal{O}(N^2N^*)$ when the number of prediction points is N^*. On the other hand, in REM reconstruction using the proposed method, only inference time for the linear term is required, as the GPR terms do not need retraining when the beam changes. Therefore, this method is efficient for REM reconstruction. Table III compares the reconstruction times for REM using the simple GPR model and the proposed method. The proposed method is shown to reduce the overall time required for REM reconstruction after a beam change to approximately 1/50 of that required by the method that simply uses GPR.

TABLE III
COMPARISON OF REM RECONSTRUCTION TIMES(SECONDS)

Method	Training Time	Inference Time
Simple GPR Model	0.690	0.417
Proposed Method	N/A	0.0195

VI. CONCLUSION

In this paper, we proposed a method to enable real time reconstruction of REMs to aim dynamic beam forming optimization in mm-wave environment. In particular, we address the spread of RSRP caused by slight differences in the position and orientation of the receiving terminal, which is particularly important for millimeter waves. GPR was used to successfully provide probability distributions. For future research, there are many areas to explore: 1) further improving accuracy, especially for NLOS locations, 2) designing a kernel suitable for multiple beam selection, 3) real-time beamforming optimization following multiple moving robots, and 4) obtaining evaluations in structures other than hallways.

ACKNOWLEDGMENT

This work was partly supported by MIC under a grant entitled “R&D of ICT Priority Technology (JPMI00316)”.

REFERENCES

[1] S. Han, C.-l. I, Z. Xu, and C. Rowell, “Large-scale antenna systems with hybrid analog and digital beamforming for millimeter wave 5g,” *IEEE Communications Magazine*, vol. 53, no. 1, pp. 186–194, 2015.
[2] A. Zanella, “Best practice in rss measurements and ranging,” *IEEE Communications Surveys & Tutorials*, vol. 18, no. 4, pp. 2662–2686, 2016.
[3] T. MATSUDA, F. ONO, and S. HARA, “Graph laplacian-based sequential smooth estimator for three-dimensional rss map,” *IEICE Transactions on Communications*, vol. advpub, p. 2020CQP0003, 2021.
[4] F. Yin and F. Gunnarsson, “Distributed recursive gaussian processes for rss map applied to target tracking,” *IEEE Journal of Selected Topics in Signal Processing*, vol. 11, no. 3, pp. 492–503, 2017.
[5] J. Zhao, X. Gao, X. Wang, C. Li, M. Song, and Q. Sun, “An efficient radio map updating algorithm based on k-means and gaussian process regression,” *Journal of Navigation*, vol. 71, no. 5, p. 1055–1068, 2018.
[6] X. Wang, X. Wang, S. Mao, J. Zhang, S. C. G. Periaswamy, and J. Patton, “Indoor radio map construction and localization with deep gaussian processes,” *IEEE Internet of Things Journal*, vol. 7, no. 11, pp. 11 238–11 249, 2020.
[7] K. J. Jang, S. Park, J. Kim, Y. Yoon, C.-S. Kim, Y.-J. Chong, and G. Hwang, “Path loss model based on machine learning using multi-dimensional gaussian process regression,” *IEEE Access*, vol. 10, pp. 115 061–115 073, 2022.
[8] D. Kodama, K. Ohira, H. Shimonishi, T. Nakahira, D. Murayama, and T. Ogawa, “Enhancing indoor millimeter radio communication: A probabilistic approach to rss map estimation,” in *2024 IEEE 21st Consumer Communications & Networking Conference (CCNC)*, 2024, pp. 241–247.
[9] S. Debroy, S. Bhattacharjee, and M. Chatterjee, “Spectrum map and its application in resource management in cognitive radio networks,” *IEEE Transactions on Cognitive Communications and Networking*, vol. 1, no. 4, pp. 406–419, 2015.
[10] K. Sato, M. Kitamura, K. Inage, and T. Fujii, “Measurement-based spectrum database for flexible spectrum management,” *IEICE Transactions on Communications*, vol. E98B, no. 10, pp. 2004–2013, Oct. 2015.
[11] H. Shimonishi, D. Kominami, Y. Ohsita, H. Yoshida, K. Nogami, D. Kanetomo, and M. Murata, “Probabilistic representation and its application of digital-twin of spatio-temporal real-world towards trustable cyber-physical interactions,” *IEEE Network*, 2024.
[12] APAL, “5g mifi hotspot,” https://www.apaltec.com/mifi/.